Supporting Information

Germanium Sulfide (II and IV) Nanparticles for Enhanced Performance of Lithium Ion Batteries

Yong Jae Cho, Hyung Soon Im, Yoon Myung, Chang Hyun Kim, Han Sung Kim, Seung Hyuk Back, Young Rok Lim, Chan Su Chung, Dong Myung Jang, Jeunghee Park, Eun Hee Cha,*, Sung Ho Choo, Min Seob Song, and Won Il Cho**

Experimental

Laser photolysis of TMG (98%, Sigma-Aldrich) and H_2S mixture was performed using an 1064 nm Nd:YAG pulsed laser (Coherent SL-10) operating with a repetition rate of 10 Hz and a pulse width of 10 ns. The precursors were degassed by several freeze (77 K)-pump-thaw cycles, then used without further purification. The precursor vapors (5-50 Torr) were introduced to a 1L volume pyrex glass reactor, equipped with a gas valve connecting to a standard vacuum line and a 2-inch diameter quartz optical window. The laser beam was focused into the closed reactor with a 10-cm focal length lens through the window. The experiment was carried using the photon energy of 0.1~0.2 J/pulse. After 1h laser irradiation, the gas products were vented and the free-standing nanoparticles (NPs) powders were collected by dispersing them in ethanol, followed by evaporation and vacuum drying at room temperature. For thermal annealing to produce the crystalline phase, the NP powders were placed in a quartz tube at 350~450 °C under vacuum for 30 min~2 h.

For electrochemical tests, the electrodes of battery test cells were made of the active material (NP), acetylene carbon black, and polyacrylic acid (PAA, 35 wt % dissolved in water; Aldrich) binder at a weight ratio of 6:2:2. The distilled water-mixed slurry was coated onto the 20 μm thick Cu foil. The coated electrode was dried at 80 °C for 12 h and then roll-pressed. The coin-type half cells (CR2032) prepared in a helium-filled glove box contained an electrode, a Li metal, a micro-porous polyethylene separator, and an electrolyte solution of 1 M $LiPF_6$ in 1:1:1 volume % of ethylene carbonate:ethyl methyl carbonate:dimethyl carbonate. The performance of the cells was examined by using a battery testing system (Maccor 4000) at a current density of 0.1 C between 0.01 and 1.5 V for 100 cycles. Cyclic voltammetry (CV) measurements were conducted (CV, Biology SAS) with a voltage range of 0.01–2.5 V at a rate of 0.1 mV/s. Electrochemical impedance spectroscopy (Solartron Multistat) was carried out by applying an AC voltage of 5 mV in the frequency range of 100 kHz to 0.01 Hz.

For the *ex-situ* XRD measurements, the cells charged or discharged to certain voltages were disassembled in a glove box and the electrodes were rinsed thoroughly with a DMC solution to remove the $LiPF_6$ salts

Figure S1. XRD patterns of Ge, Ge:*a*-GeS, *a*-GeS, and *a*-GeS_2 NPs synthesized using y = [H_2S]/[TMG]=0, 0.5, 1, and 2. The laser photolysis of TMG alone (y = 0) produced crystalline Ge NPs. The XRD peaks of the Ge NPs matched those of cubic phase Ge (JCPDS No. 04-0545; a = 5.6576 Å). The y = 0.5 sample presumably consisted of crystalline Ge and amorphous GeS NPs in a ratio of 6:4, which was estimated using EDX. Amorphous GeS and GeS_2 NPs were exclusively synthesized using y = 1 and 2, respectively. Thermal annealing at 350 °C yielded crystalline GeS and GeS_2 NPs, respectively, whose XRD patterns matched orthorhombic GeS (JCPDS No. 85-1114; a = 4.290 Å, b = 10.42 Å, c = 3.640 Å) and GeS_2 (JCPDS No. 40-0443; a = 11.72 Å, b = 22.42 Å, c = 6.871 Å), respectively.

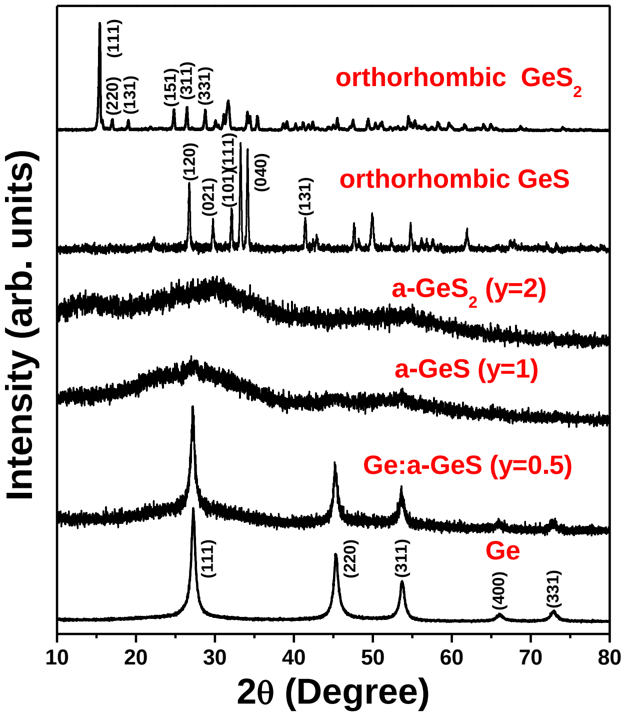

Figure S2. EDX shows 1:1 and 1:2 ratios of Ge and S elements for the (a) *a*-GeS and (b) *a*-GeS_2 NPs, respectively. (c) Survey-scan XPS of *a*-GeS_x and *c*-GeS_x (x = 1 and 2) showing the Ge and S peaks. The peak intensity of S 2*p* increases with x. The value of x is consistent with the values measured using the EDX and XRD patterns.

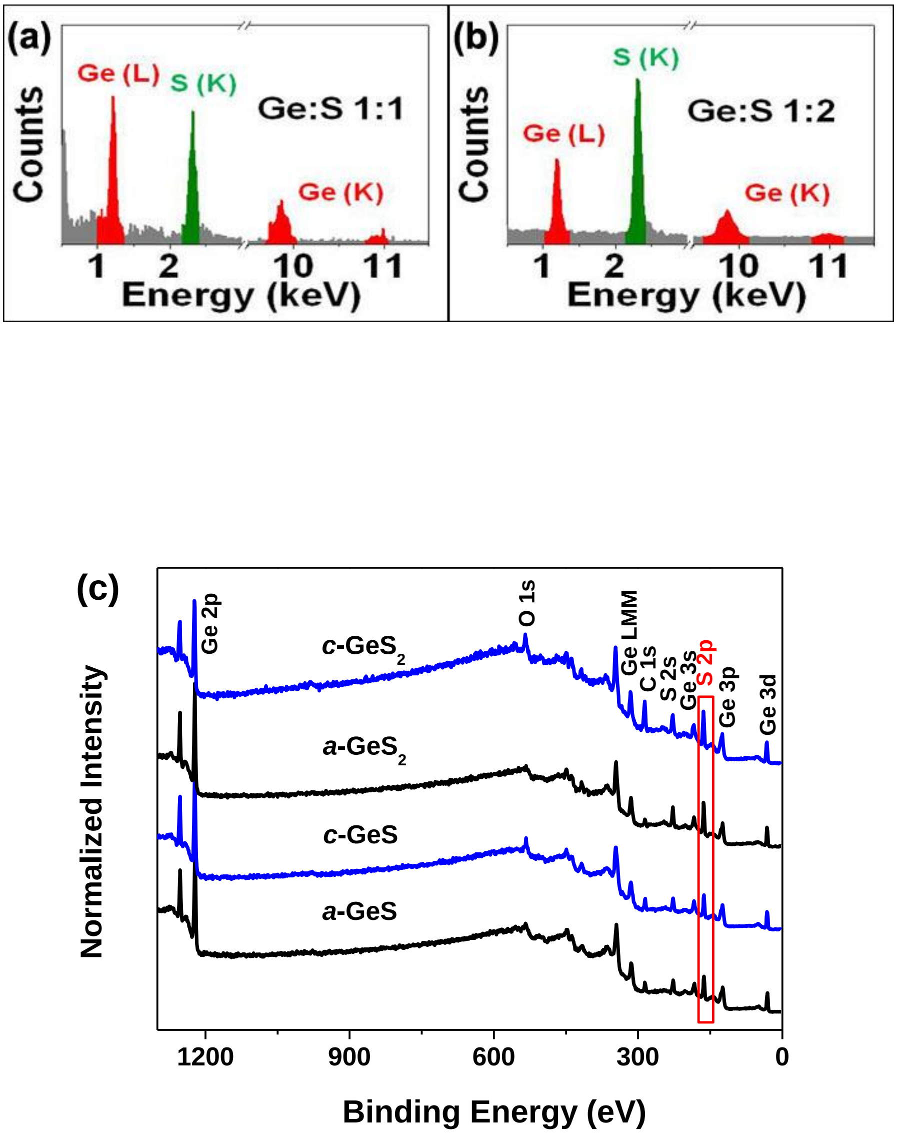

Figure S3. Charge and discharge voltage profiles of coin-type half cells using (a) *a*-GeS_2 and (b) *c*-GeS_2 NPs for 1, 2, 5, 10, 50, and 100 cycles tested between 0.01 and 1.5 V at a rate of 160 mA/g. The *c*-GeS_2 shows a plateau at ~0.9 V in the first discharge process, which is ascribed to the irreversible decomposition of GeS_2 into Ge and Li_2S; $GeS_2 + 4Li \rightarrow Ge + Li_2S$. The corresponding plateau also appears at 0.7 V in the voltage profile of *a*-GeS, at a much shorter capacity interval. Both *a*-GeS_2 and *c*-GeS_2 show the plateau region at approximately 0.2 V for all cycles, respectively, corresponding to the reversible process of lithium insertion/desertion of Ge ($Ge + xLi \rightarrow Li_xGe$).

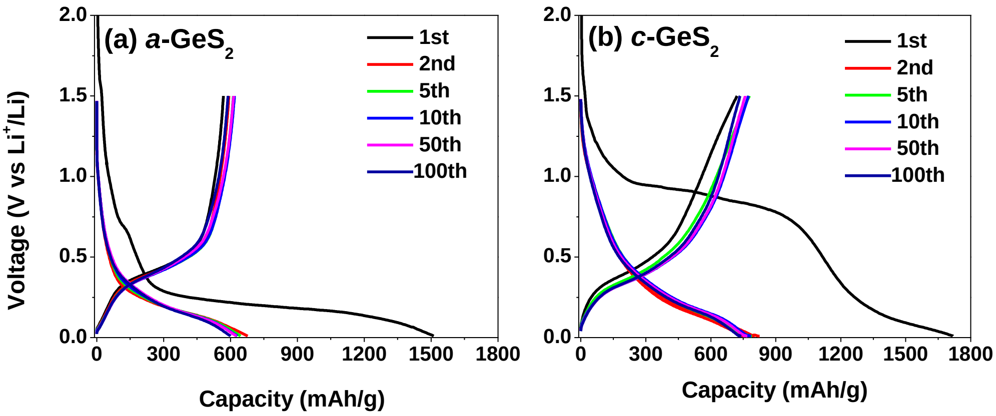

Figure S4. CV curve for (a) *a*-GeS, (b) *c*-GeS, (c) *a*-GeS_2, and (d) *c*-GeS_2 NP electrodes at a scan rate of 0.1 mVs^{-1} over the voltage range from 0.01 to 2.5 V.

The *c*-GeS exhibits the cathodic peak at 0.7 V in the first potential sweeping, which disappeared in the second sweeping. The *a*-GeS also shows the matching peak in the region between 0.6 V and 0.9 V in the first potential sweeping. We assigned these peaks to the decomposition of GeS into Ge and Li_2S. Both *a*-GeS and *c*-GeS show a pair of redox current peaks at potentials of around 0.35 V and 0.40 V, respectively. Therefore, it can be regarded as the signature of the alloying (cathodic scan)/dealloying (anodic scan) of lithium from Ge: $Ge + xLi \leftrightarrow Li_xGe$.

c-GeS_2 shows a strong cathodic peak at 0.9 V in the first potential sweeping, which is assigned to the decomposition of GeS_2 into Ge and Li_2S: $GeS_2 + 4Li \rightarrow Ge + 2Li_2S$. The cathodic peak shifted to the higher voltage region with a reduced intensity in the subsequent sweeping. We tentatively assigned it to the irreversible formation of Li_xGeS_2 and/or its decomposition into Ge and Li_2S: $Li_xGeS_2 + (4\text{-}x)Li \rightarrow Ge + 2Li_2S$. The *a*-$GeS_2$ exhibits the weak cathodic peak over a wide potential rage of 0.6~1.5 V in the first potential sweeping. The *a*-GeS and *c*-GeS show a pair of redox current peaks at potentials of around 0.35 V and 0.40 V, respectively, which is ascribed to the alloying/dealloying of lithium from Ge: $Ge + xLi \leftrightarrow Li_xGe$.

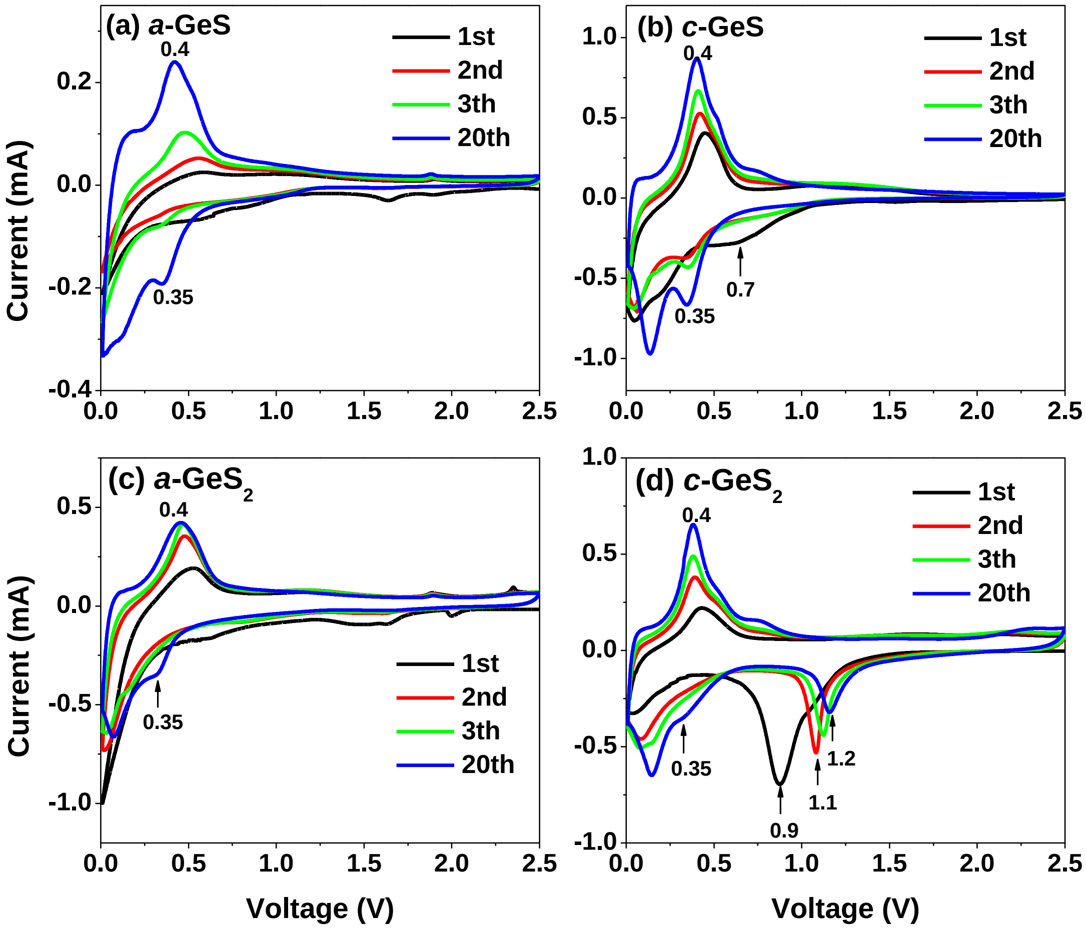

Figure S5. Nyquist plots of *a*-GeS, *c*-GeS, *a*-GeS_2 and *c*-GeS_2 NP before cycling (state of charge (SOC) = 0%). All consist of one semicircle in high frequency region and a straight line in the low frequency region. The semicircle portion is related to the reaction in the electrode/electrolyte interface, which reflects the charge transfer impedance and solid electrolyte interphase (SEI) impedance. The diameter of the semicircle equals the charge transfer resistance, and its intercept with the Z_{real} axis corresponds to that of SEI. Amorphous NPs possess has the higher charge transfer resistance than the crystalline NPs, which may be attributable to the slower Li^+ ion transfer rate

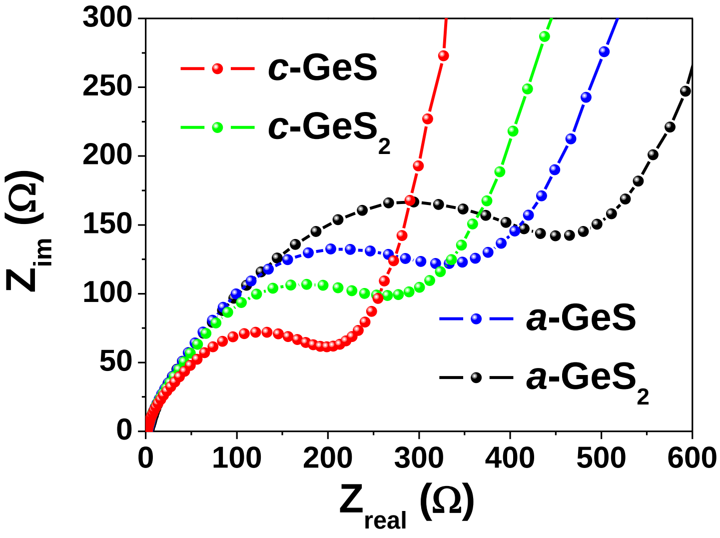

Figure S6. XRD pattern of *a*-GeS electrodes after first and third discharge (after fully charged to 1.5 V), and after 100 cycles. As the cell is discharged to 0.01 V, the new peaks at 20.2°, 32.3° and 35.6° emerge, corresponding to (110), (201) and (211) of tetragonal Ge (JCPDS No. 72-1425; a = 5.93 Å and c = 6.98 Å), respectively. These peaks remain as a main feature after the cell is 100 th charged.

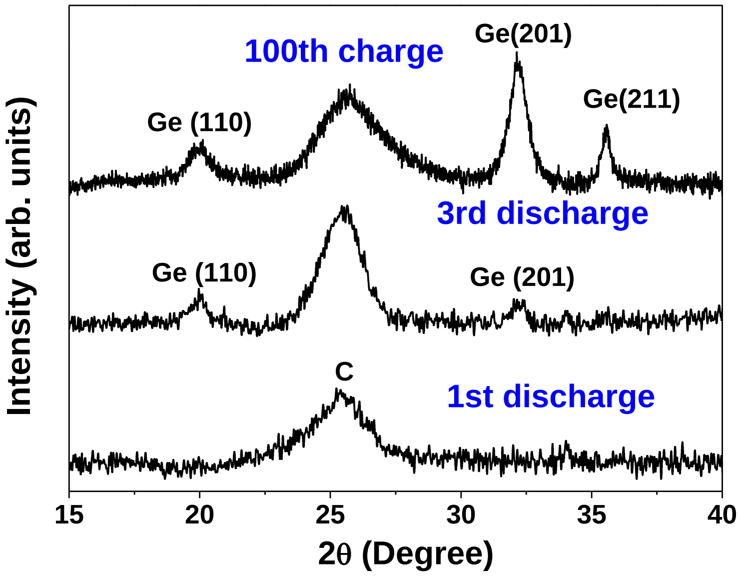

Figure S7. HRTEM image and intensity line profiles of NPs (sampled from the fully charged cell after 50 cycles) reveal that the *d*-spacing of (201) and (111) planes is 2.7 and 3.6 Å, respectively, which is close to that of tetragonal Ge.